[5] Page, W. A., Compton, D. L., Borucki, W. J., Ciffone, D. L., and Cooper, D. M., "Radiative Transport in Inviscid Nonadiabatic Stagnation-Region Shock Layers," *AIAA Progress in Astronautics and Aeronautics: Thermal Design Principles of Spacecraft and Entry Bodies*, Vol. 21, edited by J. T. Bevans, Academic Press, New York, 1969, pp. 75–114.

[6] Chin, J. H. and Hearne, L. E., "Shock-Layer Radiation for Sphere-Cones With Radiative Decay," *AIAA Journal*, Vol. 2, No. 7, July 1964, pp. 1345–1347.

[7] Coleman, W. D. et al., "Effects of Environmental and Ablator Performance Uncertainties on Heat-Shielding Requirements for Hyperbolic Entry Vehicles," *Journal of Spacecraft and Rockets*, Vol. 5, No. 11, Nov. 1968, pp. 1260–1270.

[8] Wilson, K. H., "Stagnation Point Analysis of Coupled Viscous-Radiating Flow With Massive Blowing," CR-1548, June 1970, NASA.

[9] Wilson, K. H., "Massive Blowing Effects on Viscous, Radiating Stagnation Point Flow," AIAA Paper 70-203, New York, 1970.

[10] Vulliet, W. G., Sand, S. J., and Findley, W. B., "Sputter Treatment of Ablation in the Atmosphere of Jupiter," Final Report, JPL Contract 952480, Gulf General Atomics, June 30, 1969.

[11] Adams, M. C., "Recent Advances in Ablation," *ARS Journal*, Vol. 29, No. 9, Sept. 1959, pp. 625–632.

[12] Canning, T. N., Tauber, M. E., and Wilkins, M. E., "Review of Recent Ballistic Range Boundary-Layer Transition Work on Ablating Bodies at Ames," *Proceedings—Boundary Layer Transition Study Group*, Aerospace Corp., San Bernardino, Calif., July 11 and 12, 1967.

[13] Moyer, C. B. and Rindal, R. A., "An Analysis of the Coupled Chemically Reacting Boundary Layer and Charring Ablator," Rept. 66-7, March 1967, Aerotherm Corp.

[14] *JANAF Thermochemical Tables*, The Dow Chemical Co., Aug. 1965.

[15] Duff, R. E. and Bauer, S. H., "The Equilibrium Composition of the C/H System at Elevated Temperatures," LA-2556, Sept. 1961, Los Alamos Scientific Lab.

[16] Allen, H. J. and Eggers, A. J., "A Study of the Motion and Aerodynamic Heating of Missiles Entering the Earth's Atmosphere at Supersonic Speeds," TN 4047, 1957, NACA.

JUNE 1971 J. SPACECRAFT VOL. 8, NO. 6

Ablative Material Tests under Transient Heating Simulating Ballistic Re-Entry

BARRY J. MITCHEL*
Avco Systems Division, Wilmington, Mass.

The ablative and insulative performance of reference silica phenolic and carbon phenolic heat shield materials was investigated under simulated trajectory heating characteristic of a medium-performance ballistic vehicle. A 10-Mw, 4-arc plasma-jet facility generated a stepwise-transient, supersonic, turbulent heating environment in a pipe specimen configuration. Agreement between experimental and theoretical values for surface and internal temperatures, surface recession, char depth, and weight loss was generally good for the silica phenolic, except during terminal heating when the melt removal rate was increased rapidly by aerodynamic shear stress. Agreement also was good for carbon phenolic with a 30° cloth layup, except near peak heating when carbon sublimation became the dominant ablative mechanism. However, the same material with a 90° layup was susceptible to mechanical erosion.

Nomenclature

A = turbulent heating correlation factor
C_2 = second radiation constant = 2.59×10^4 μ-°R
c = specific heat
g = force-mass conversion constant = 32.174 lbm-ft/sec^2-lbf
H = total enthalpy
ΔH = enthalpy increase during reaction
h = convective heat-transfer coefficient
k = thermal conductivity
M = Mach number
m = sonic-throat mass flux
q,q^* = heat flux and heat of ablation
Re = Reynolds number
r = radial distance
S = heat-sink capacity at cooled surface
St = Stanton number
s = stoichiometric ratio for combustion
T = temperature
t = time
U = gas flow speed
V = flight speed
v = surface or char-front speed
w = weight
W = mass fraction of oxygen in gas stream
α,ϵ = absorptance and emittance
γ = flight path angle
δ = char depth
η = transpiration blocking coefficient
θ = cone half-angle
λ = wavelength of radiation
ν = 0, 1, or 2 for slab, cylinder, or sphere
ρ = material density
ρ_g = change of density = $\rho_v - \rho_c$
σ = Stefan-Boltzmann radiation constant = 0.476×10^{-12} Btu/sec-ft^2-°R^4
τ = aerodynamic shear stress
Φ = transpiration-blocking function

Subscripts

A,a = ablation conditions, ambient conditions at cooled surface
B = brightness
C = cold-wall convective
c,d = charred material and decomposition (charring) process
E = re-entry altitude = 300 kft
e,g = external gas stream and pyrolysis gas

Presented as Paper 69-150 at the AIAA 7th Aerospace Sciences Meeting, New York, January 20–22, 1969; submitted March 3, 1969; revision received January 15, 1971. This work was supported by Air Force Materials Laboratory, Air Force Systems Command through Contract AF33(615)-3923 under the technical guidance of R. W. Farmer (MANC). The author wishes to thank many associates, including H. E. Hoercher, P. J. Roy, F. L. Tempesta, and R. Shaw Jr.

* Senior Consulting Scientist, Hyperthermal Simulation and Instrumentation Section, Material Applications Department. Member AIAA.

i = induction of steady-state ablation
I = interface of decomposition (char front)
L = cooled (rear) surface
R = incident radiative
T = true value after emittance correction
v,w = virgin material and heated (front) surface
x = distance along pipe axis
0 = initial conditions
λ = monochromatic wavelength

Introduction

TRAJECTORY heating simulation is a necessary final step in the comprehensive evaluation of ablative materials for increasingly demanding heat-shielding applications. Phenomena can be observed that do not occur during steady-state heating, e.g., surface recession more rapid than char-front propagation, liquid layer removal faster than subsurface melting, or overthick char-layer failure under increasing stresses. Predictive ablation models, in which certain parameter values are necessarily based on steady-state tests, can be validated or modified before actual designs are finalized.

This paper presents results of an early series of trajectory-simulation tests. Other tests in a time-varying environment, reported simultaneously,[1] comprised a systematic phenomenological study, in contrast to the design-application study presented here. Recent improvements in specimen design[2] permit better simulation of fabric layup, and more comprehensive measurements of ablative performance, than were possible in these early tests.

In the present work, a sidewall location on a slender conical vehicle was chosen for ballistic trajectory simulation. The four arcs tributary to the Avco 10-Mw arc facility[3] plenum chamber were programed to fire and shut down in sequence to generate a 6-step approximation to the calculated transient environment. Although the simulation was not exact, it did allow for initial thickening of the char, followed by a rapid increase of shear stress, pressure, and heat flux. The results were compared with theoretical predictions of a computerized charring-ablator model (see Appendix) which did not account for mechanical ablative mechanisms. In cases where significant discrepancies occurred between theory and experiment, interrupted trajectory runs were made to isolate the trajectory step(s) causing the adverse ablative phenomena and to examine the char layer prior to each critical step. Steady-state runs also were made at selected trajectory points for comparison.

Experimental Program

Materials, Specimen Preparation, and Specimen Measurements

Fabrication data for the test materials—a silica cloth phenolic (Avco X6000A) and a carbon cloth phenolic (R6300)—are given in Table 1. Specimens from the same material batches had been evaluated in three laminar, low-shear, stagnation-point environments in another phase of this program.[4] Two fabric ply orientations, parallel and normal to the heated surface, were compared, and no important effects of ply orientation were found for either material in the low-shear environments. Therefore, the normal orientation was selected for the supersonic-pipe specimens because of its simplicity of fabrication and machining. These specimens were machined in two pieces, which were housed in an uncooled copper sleeve (Fig. 1). The upstream end was butted directly against the facility's 0.8-in.-i.d. sonic nozzle, and the downstream or exit end was retained by a stainless steel plate; O-rings were used in three places to prevent any gas leakage through joints. One specimen of the carbon phenolic material was fabricated in a conical dixie-cup layup with plies at 30° to the axis and pointing in the flow direction.

Four specimens of each material were instrumented with three chromel-alumel thermocouples in the downstream test section. Each junction was formed by resistance-welding a 1-mil platinum wire across the flat ends of 5-mil chromel and alumel wires contained in a 30-mil-diam vitrified alumina sheath. Each sensor was cemented into a flat-bottom hole drilled parallel to the pipe axis (Fig. 1) to minimize temperature disturbances caused by dissimilarity between the sensor and test material.[5]

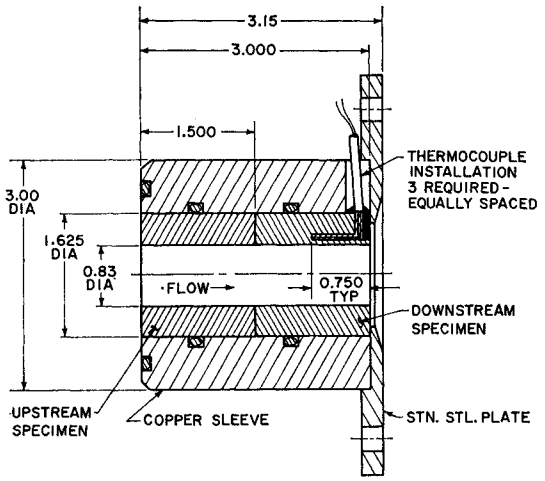

Fig. 1 Test specimen showing thermocouple installation.

Pretest and post-test measurements of length and outside diameter were made with a C-type micrometer gage, and the inside diameter was measured by a special spring-loaded caliper tool. Pretest and post-test weights were measured with thermocouples installed, since there was negligible weight loss of the thermocouple lead wires during a test. Average char depth over each sectioned downstream specimen was measured with the aid of a magnifying lens. In general, the silica phenolic samples had sharp char-layer boundaries, whereas the carbon phenolic samples displayed pyrolysis zones of discernible thickness (0.020–0.040 in.).

Experimental Configuration and Environment Calibration

The arc-heated plasma flowed through the pipe specimen (Fig. 2), producing a turbulent high-shear environment. A Thermodot recording pyrometer, focused on a small segment of the heated inner surface of the pipe specimen, provided a continuous record of the brightness temperature at a wavelength of 0.80 μ. Color films were obtained with a Bell and Howell 16-mm camera at 64 frames/sec. Internal temperatures were recorded during hyperthermal exposure and for an additional 20 sec during the ensuing thermal-soak period.

Since the geometry of the pipe permitted radiative exchange from one portion of the pipe to another, the radiation sensed by the pyrometer consisted of both reflected and emitted components. To obtain true surface temperature, therefore, the brightness temperature correction was made using the following formula derived from the Wein approximation

Table 1 Test materials[a]

Material code	Reinforcing agent	Resin[b] content, pbw	Bulk density, g/cm³
X6000A	Astrosil 84 silica cloth (J. P. Stevens Co.)	37	1.65
R6300	Pluton B-1 carbon cloth (3M Co.)	41	1.46

[a] Molded at 600 psia for 8 hr at 175–325° F. Postcured at 350° F for 16 hr.
[b] Monsanto SC-1008 phenolic; pbw = percent by weight.

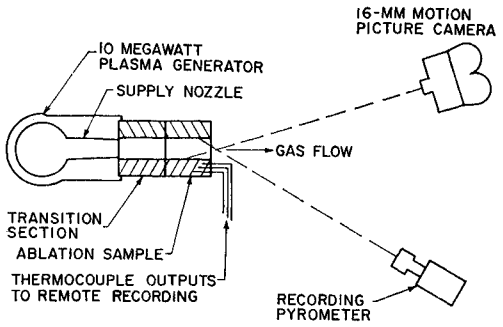

Fig. 2 Experimental configuration.

to Planck's spectral distribution law:

$$1/T_T = 1/T_B + (\lambda/C_2) \ln \epsilon_\lambda \quad (1)$$

where ϵ_λ is the effective spectral emittance of the pipe.

The spectral emittance of the test materials was not known very accurately, but was presumed to be on the order of 0.80 at 0.80 μ, yielding 0.93 for ϵ_λ at the aiming point of the pyrometer.[6] Corrections to the recorded T_B thus were rather small, ranging from 45° R at T_B = 4500° R to 110° R at T_B = 7000° R.

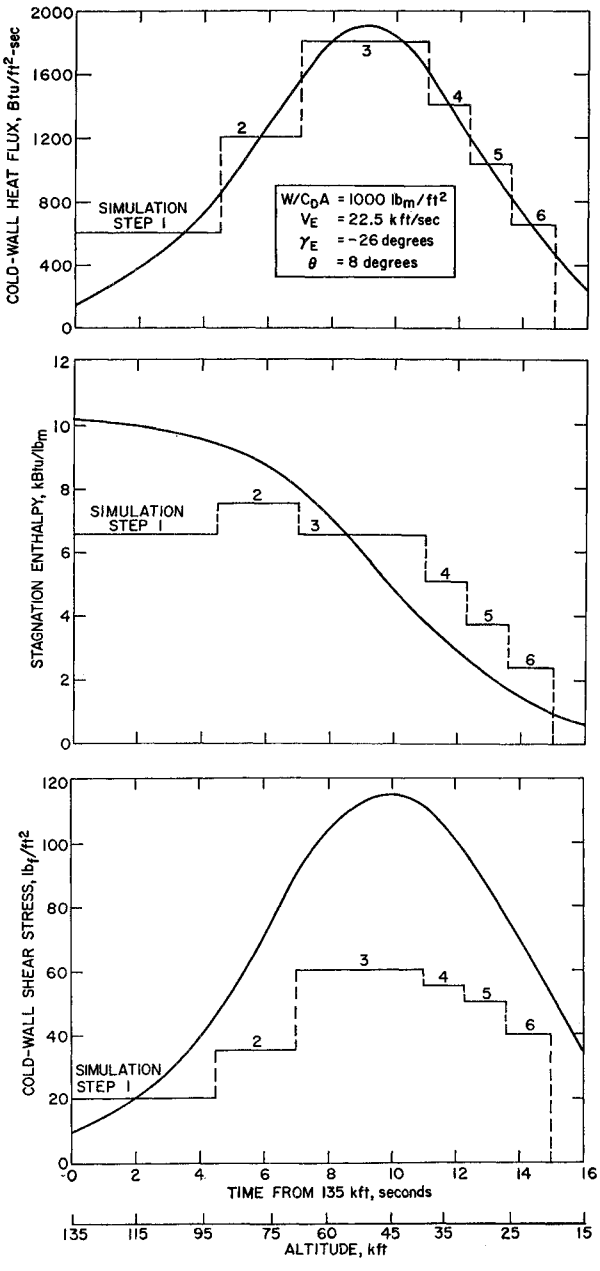

Fig. 3 Transient environment of typical ballistic vehicle.

The environments were calibrated by means of copper pipe specimens with pressure and heat-flux instrumentation. The pressure data revealed an initial undershoot and partial recovery of the pressure in the upstream section, followed by nearly uniform pressure in the downstream section. The heat flux (q_w) was measured by means of transient null-point copper calorimeters[7,8] at several locations. These data showed that q_w was nearly uniform over the downstream section, and could be correlated with air flow rate and total enthalpy in the form

$$q_w = Am^{0.8}(H_e - H_w) \quad (2)$$

in which the best fit was obtained with $A = 7.9 \pm 0.6 \times 10^{-3}$ (lbm-ft^{-2}sec^{-1})$^{0.2}$. Equation (2) corresponds to the nondimensional relationship, $St = f(M)Re_x^{-0.2}$, for fully developed turbulent heat transfer. For each specimen test, the cold-wall (H_w = 0) heat flux was calculated from Eq. (2) using the measured values of H_e and m.

The aerodynamic viscous shear stress acting on the inner surface of a nonablating pipe was estimated by means of Reynolds' analogy

$$\tau_w = q_w U_e/(H_e - H_w)g = Am^{0.8}U_e/g \quad (3)$$

The bulk flow speed U_e in the pipe was estimated on the basis of isentropic expansion from the measured plenum pressure to the measured downstream-section pressure.

Following the test series, additional pressure and heat-flux surveys were made in contoured copper pipes representing three typical ablated pipe specimens. The resulting changes of the correlation constant A in Eq. (2) were less than the experimental scatter. For practical purposes, therefore, the cold-wall q_w was unaffected by surface recession. This apparent contradiction of other data for smooth nozzles[9] could be attributed to the nonuniform contour. The backward-facing step at the sonic throat tripped the boundary layer, which developed from the reattachment point. Erosion caused three effects on q_w at any fixed station, viz., increased M, reduced freestream flux, and reduced Re_x due to both the increased diameter and a downstream shift of the reattachment point. These effects fortuitously cancelled each other for the typical ablated contours.

Trajectory Simulation

The reference trajectory was that of a typical slender, low-drag, long-range ballistic vehicle, with the reentry parameters given in Fig. 3. It was computed by standard methods, neglecting the effects of ablation on the ballistic coefficient. The histories of stagnation enthalpy, cold-wall heat flux, and shear stress were calculated for the 1-ft station on the cone, neglecting blunting of the cone tip.[10] Turbulent heating rates were assumed throughout the re-entry history. The 6-step sequence used to approximate this transient environment is shown in Fig. 3. To account approximately for early heating at levels too low to be simulated, the duration of step 1 was chosen so that the integrated heat fluxes for the actual and simulated trajectories matched at the end of this step. The duration of each additional step then was chosen to continue matching the integrated heat fluxes.

The real-time character of the simulation assured that the competing heat-shielding mechanisms of surface vaporization, internal charring, and energy storage were in realistic balance at all times. It is noted, however, that the pipe configuration inhibited radiative cooling; a convective-radiative environment existed in which the radiative component was material-dependent. The resulting increase of environmental severity was greater for the carbon phenolic than for the silica phenolic.

Experimental Results and Comparison with Theory

Silica Phenolic (X6000A) Specimens

This material ablated smoothly and predictably in all test environments by a melting-vaporizing process that was clearly visible in the color movies. At the most severe condition of shear stress and heat flux (step 3), the molten surface layer was very thin and coherent; in contrast, at the low-flux, low-enthalpy condition (step 6), the liquid flowed in large individual droplets. Over the entire range of test conditions, T_T during ablation varied less than 600° R, indicating a vapor-pressure-controlled ablative process. No spalling or mechanical erosion was noted.

Since the supersonic character of the flow set a limit on surface recession, pairs of specimens shared the full trajectory heat load. Division at the time of maximum q_w was advantageous, because after a short induction time (theoretically 0.3 sec)[11] the second specimen approached a steady-state ablation condition identical to the terminal condition of the first. After a suitable linear translation, the second test could be considered as a continuation of the first.

Table 2 presents test conditions, trajectory step durations (where applicable), and representative values of T_T for each step. Typical sectioned silica phenolic specimens are shown in Fig. 4. Experiment and theory are compared in Table 2 for weight loss, in Fig. 5 for surface recession Δr and char depth δ, and in Figs. 6 and 7 for internal temperatures during two complementary half-trajectory tests. The agreement was generally satisfactory, with the following two exceptions. In the second half trajectory, the data agreed well with theory on the basis of Δr, δ, and over-all weight loss Δw (Table 2 and Fig. 5). However, the color movies and the internal temperature data (Fig. 7) indicated that the surface recession rate v_w on step 6 was higher than predicted. Since the predictions had been made on the assumption of a constant vaporized fraction of the melt layer, this discrepancy was attributed to rapid melt-removal and slow vaporization under relatively high shear stress and low heat flux.[12] In the first half trajectory, Δr and internal temperature data (Figs. 5 and 6) agreed well with theory through step 2. During step 3, however, a v_w well below the theoretical rate was indicated by the subsequent internal temperature data, and was confirmed by final measurements of Δr, δ, and Δw (Fig. 5 and Table 2). The reason for this discrepancy is not well understood, but has been ascribed to reduced q_w, because the internal diameter profiles[4] did not conform to the general pattern for which contoured calorimeters showed constant q_w (see the preceding section, Experimental Configuration and Environment Calibration).

In summary, agreement between low-shear theory and experiment was very good for silica phenolic with two notable exceptions. One discrepancy indicated that the heat of ablation could be reduced under moderate-to-high shear forces if the hot-wall heat flux were insufficient to vaporize the flowing liquid layer. This effect could be important during the terminal flight period for ballistic re-entry vehicles. The other discrepancy was attributed to a deviation from nominal test conditions due to an unusual but reproducible contour of two ablated pipes.

Carbon Phenolic (R6300)

The eight carbon phenolic specimens with plies oriented normal to the gas-flow direction displayed a susceptibility to mechanical erosion and spalling. At the less severe test conditions, the spalling was random and infrequent, and the resulting wide but shallow depressions often were smoothed by subsequent oxidation. At the more severe conditions, in contrast, a continuous stream of small solid particles was eroded from the entire surface area, and small depressions tended to grow. The resulting surfaces were very irregular.

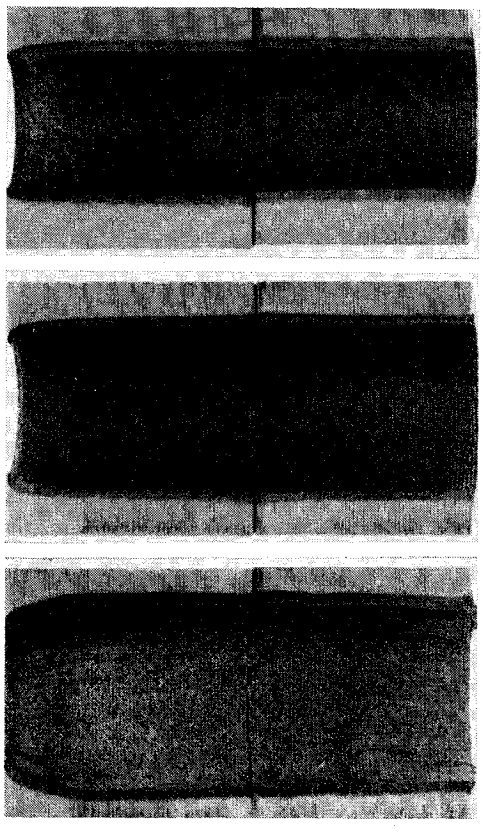

Fig. 4 Sectioned silica phenolic specimens representing (top to bottom) early, peak, and terminal heating periods. Air flow was left to right.

Experiment and theory are compared in Fig. 8 for Δr and δ. Because of mechanical erosion, the agreement was generally poor except during step 1 and perhaps step 2 (i.e., for 7 sec). Mechanical erosion was even more severe in subsequent steady-state heating tests for step 2 or 3, i.e., sudden heating was worse than progressively increased heating.[4] This result might be explained by either 1) relief of thermal gradients and stresses in the established char layer by internal transpiration cooling, mass-injection blocking, and other mechanisms, or 2) greater strength of the mature char layer as a result of pyrolytic graphite deposition on the fibers. However, the actual cause could not be established from the test data.

Mechanical erosion was not observed in earlier tests which included carbon and graphite reinforcing fabrics in the 90° orientation[13] and were conducted in a steady-state environment corresponding to step 3 of the present trajectory simula-

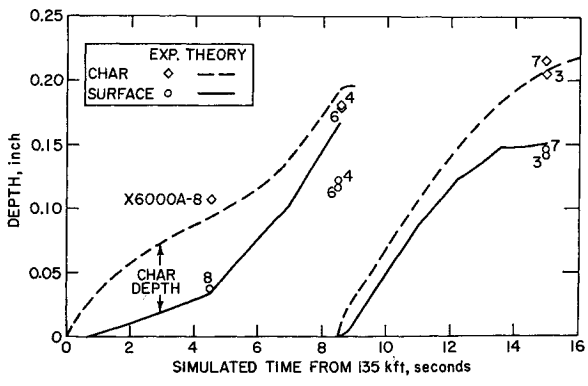

Fig. 5 Silica phenolic ablation and char depth.

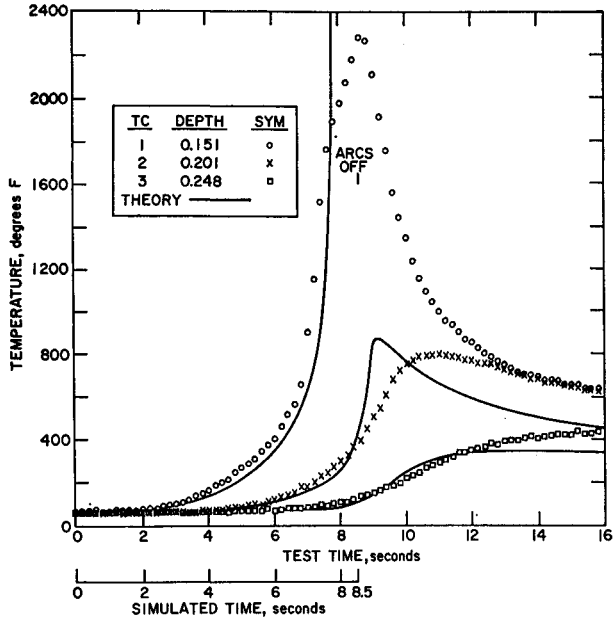

Fig. 6 Silica phenolic temperature response until time of peak heating (cooling data are incidental).

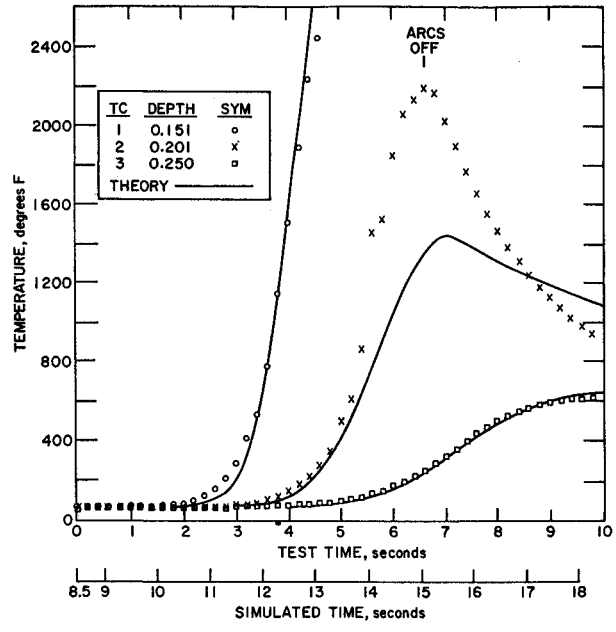

Fig. 7 Silica phenolic temperature response after peak heating (add 0.178 to depths, see text and Fig. 5).

tion. Therefore, the present erosion results do not apply generally to materials with carbonaceous reinforcement.

A single specimen with 30° ply orientation was fabricated by the so-called dixie-cup technique of stacking conical plies, impregnating with resin, and press-molding. It was machined so that the cone vertices lay along the pipe axis, pointing in the flow direction. This specimen, exposed to a full simulated trajectory, survived with no evidence of spalling or mechanical erosion. The total Δr and final δ agreed well with theoretical predictions (Fig. 8 and Table 2) based on diffusion-limited oxidation. The small differences could be attributed to some sublimation of carbon on step 3, when T_T exceeded 7000°R. Examination of the sectioned specimen revealed a smooth internal surface and relatively uniform char depth, in contrast to the 90° layup material (Fig. 9).

Conclusions

1) A transient environmental history, typical of a sidewall location on a slender vehicle, was simulated in real time in a high-power multi-arc heater, by programing air flow and power to the four arcs in stepwise fashion.

2) Data for the silica phenolic (X6000A) specimens generally agreed well with predictions of a charring-ablator computer program using steady-state heat-of-ablation data from low-shear turbulent pipe tests. Ablation efficiency was

Table 2 Summary of test data

Specimen code	Run type[a]	Step no.	Δt, sec	q_c, Btu/ft²-sec	H_e, Btu/lbm	T_T, °R[b]	Δr, in.[c]	δ_c, in.[c]	Wt. loss, gm Exp.	Wt. loss, gm Theo.
X6000A-1	SS	3	5.54[d]	1897	6810	5000	0.195	0.025	27.1	27.2
X6000A-5	SS	3	5.11	1883	6740	4910	0.185	0.03	25.5	24.2
X6000A-8	PT1	1	4.45	592	6440	4650	0.035	0.075	6.4	5.5[e]
X6000A-4	PT1	1	4.30	576	6340	4550				
		2	2.60	1190	7520	4880				
		3	1.67	1742	6310	4780	0.120	0.055	17.3	21.8
X6000A-6	PT1	1	4.30	595	6470	4470				
		2	2.70	1159	7250	4830				
		3	1.58	1779	6410	4800	0.115	0.06	16.4	21.8
X6000A-3	PT2	3	2.50	1897	6810	4950				
		4	1.28	1390	4990	4830				
		5	1.63	1014	3640	4780				
		6	1.15	685	2460	4550	0.140	0.065	20.3	21.0
X6000A-7	PT2	3	2.51	1949	6980	4900				
		4	1.35	1403	5020	4760				
		5	1.42	1026	3680	4720				
		6	1.39	678	2430	4440	0.145	0.07	22.4	21.0
R6300-9[f]	FT	1	4.40	632	6880	5410				
		2	2.54	1310	8190	6620				
		3	4.10	1812	6510	7080				
		4	1.48	1315	4720	6670				
		5	1.06	986	3540	6290				
		6	1.43	667	2400	5280	0.105	0.18/ 0.21	22.4	17.0

[a] SS—steady state; PT1—partial trajectory, first half; PT2—partial trajectory, second half; FT—full trajectory.
[b] Refer to Eq. (1).
[c] Average value over downstream test section.
[d] Timer was set incorrectly; nominal time was 5.0 sec.
[e] Does not include additional charring during thermal soak.
[f] 30° fabric layup.

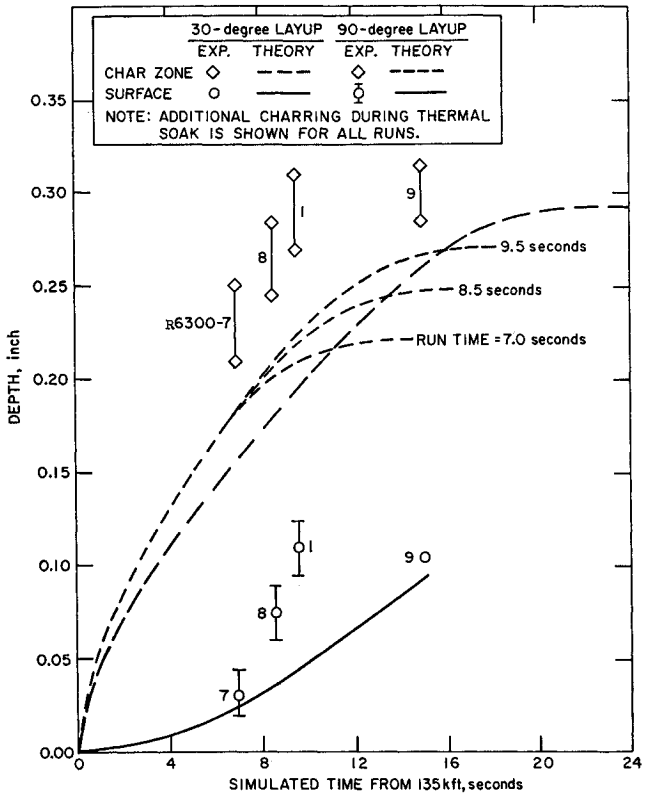

Fig. 8 Carbon phenolic ablation and char depth.

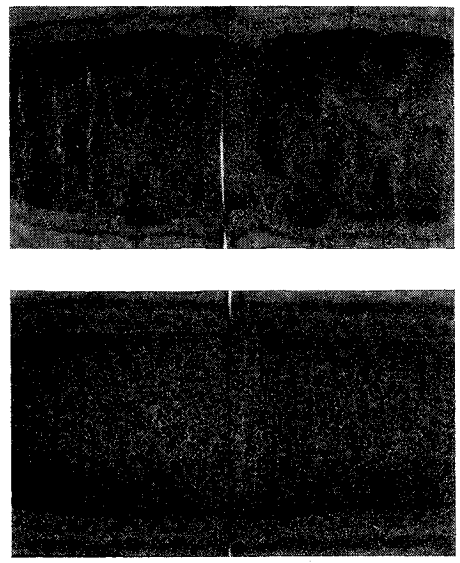

Fig. 9 Sectioned carbon phenolic specimens representing terminal heating period (top, 90° layup; bottom, 30° layup). Air flow was left to right.

not affected by shear stresses up to 60 lbf/ft² when accompanied by high heat flux. Performance was deteriorated during terminal flight at low hot-wall heat flux, due to increased liquid run-off under shearing forces.

3) Resistance of the carbon phenolic (R6300) to mechanical removal depended upon orientation of fabric plies: the 90° orientation was mechanically eroded; in contrast, the 30° orientation was not affected by shear stresses up to 60 lbf/ft², and ablative performance over the full simulated trajectory agreed well with predictions of the charring-ablator program.

4) Ablation model improvements and supporting data are required in two areas: sublimation of carbonaceous materials near peak heating, and liquid shearing from siliceous materials during terminal ballistic flight. Conventional q^* theories are not adequate for heat-shield design in these critical flight regimes.

Appendix: Charring-Ablator Computer Model

In the thermophysical model the material can exist in only two conditions, virgin and fully charred. The char front or char-virgin interface is characterized by the fixed temperature T_d and the enthalpy increase ΔH_d for the endothermic decomposition of a unit weight of virgin material. Gaseous products transpire through the char matrix to the heated surface in a direction opposite to the heat flow. The mathematical model for the internal processes was presented elsewhere.[4,14] The particular surface-chemistry models for the tested materials are presented below.

The material is heated by convection and/or radiation uniformly over the moving surface $r = r_w(t)$ and is cooled actively or rejects heat passively over the fixed surface $r = r_L$. Convective heating is provided by an attached boundary layer, assumed to be transparent and nonradiating. The surface energy balance is expressed by

$$(1 - H_w/H_e)\Phi q_C - \rho_c v_w \Delta H_c - \rho_g v_I (r_I/r_w)^p \Delta H_g + \alpha_w q_R = \epsilon_w \sigma T_w^4 - (k\partial T/\partial r)_{r=r_w} \quad (4)$$

In the pipe tests, $q_R \propto T_w^4$, so the radiation absorption and emission terms are combined into a single term, using an effective value of ϵ_w based on view-factor calculations. The blocking function Φ is assumed to be a linear function of the mass injection rates, i.e.,

$$\Phi = 1 - [\rho_c v_w \eta_c + \rho_g v_I (r_I/r_w)^p \eta_g] H_e/q_C \quad (5)$$

with the restriction $\Phi \geq 0$. The use of Eqs. (4) and (5) differs for the silica-reinforced and carbon-reinforced materials, as follows.

For the silica phenolic, the classical concept of an ablation temperature T_A is introduced, i.e.,

$$T_w(t) = T_A \text{ when } v_w > 0 \quad (6)$$

$$T_w(t) < T_A \text{ when } v_w = 0 \quad (7)$$

Before ablation begins, Eqs. (4) and (5) determine T_w with $v_w = 0$. During ablation, Eqs. (4) and (5) determine v_w with $T_w = T_A$. A positive value is assigned to ΔH_c corresponding to the latent heat of vaporization of the silica. This simplification omits the effects of aerodynamic shear and pressure gradient on the flowing liquid layer.[12]

For the carbon phenolic, the char removal mechanism is assumed to be oxidation, limited by boundary-layer diffusion or turbulent transfer. The incoming flux of oxygen is reduced by a countercurrent of the products of pyrolysis and char combustion. The surface recession rate v_w is determined, independently of the energy balance, by the following equation:

$$W_e \Phi q_C/H_e = \rho_c v_w s_c + \rho_g v_I (r_I/r_w)^p s_g \quad (8)$$

with the restriction $v_w \geq 0$. Equation (4) then determines the surface temperature with no upper limit.

The rear face of the ablator is assumed to be bonded to a thin, high-conductivity plate whose uniform temperature varies only with time. Heat transfer between the plate and an ambient medium at constant temperature occurs by convection and radiation. The boundary condition is written as follows:

$$h_L(T_a - T_L) + \sigma(\alpha_L T_a^4 - \epsilon_L T_L^4) = (S\partial T/\partial t + k\partial T/\partial r)_{r=r_L} \quad (9)$$

Table 3 presents the input values used in the theoretical heat-shield trajectory calculations. To avoid unnecessary complications, all properties were assigned temperature-inde-

Table 3 Input values for charring-ablator model

Symbol	Units	(90°) X6000A	(30°) R6300[a]
ρ_v	lbm/ft³	103.0	91.2
c_v	Btu/lbm-°R	0.3	0.35
k_v	Btu/hr-ft-°R	0.4	0.6
T_d	°R	1460	1460
ΔH_d	Btu/lbm	185	205
ρ_c	lbm/ft³	82.4	68.4
c_c	Btu/lbm-°R	0.25	0.35
c_g	Btu/lbm-°R	0.45	0.45
k_c	Btu/hr-ft-°R	0.6	1.0
T_A	°R	4800	...[b]
ΔH_c	Btu/lbm	1330	−3800
s_c	lbm O_2/lbm	...[b]	1.13
η_c, η_g		0.3	0.3
ϵ_w		0.15[c]	0.15[c]
ϵ_L, α_L		1.00	1.00
h_L	Btu/hr-ft²-°R	120	120
r_w	in.	0.414	0.414
r_L	in.	0.812	0.812

[a] Properties for 90° layup differ only in $k_v = 0.9$ and $k_c = 1.5$.
[b] Not used in model for this material.
[c] Effective value based on view factor.

pendent values. (More recent data indicate that temperature dependence is important, but the present theoretical results are not affected seriously.) The primary sources of thermophysical data were as follows. The input values of ρ_v were the mean values for the pipe specimens. The ρ_c of X6000A was obtained from TGA data and microtome measurements of arc-test specimens of similar resin content and density.[15] The ρ_c of R6300 was estimated from analogous data for other test specimens.[16] Degradation data for SC-1008 phenolic resin and the specific heat of its pyrolysis gases were taken from Ref. 17. Because the principal escaping gas products are H_2 and CO, which do not oxidize at high temperatures,[17,18] ΔH_g and s_g were set equal to zero.

Data for the silica phenolic were taken primarily from Ref. 15; k_c was obtained by a linear extrapolation of the low-temperature data to 1500°F. The T_A for the pipe tests was estimated from the screening test results in two laminar stagnation-point environments of comparable heat flux and enthalpy levels.[4] The effective heat of vaporization was obtained by extrapolating q^* vs H_e data for laminar flow to $H_e = H_w$, and then subtracting the sensible energy based on the other properties. The primary source of property data for carbon phenolic was Ref. 16, which includes data for k for 0°, 30°, and 90° orientations; the measured values were increased slightly to account for the mean density difference between the arc-test specimens and the conductivity specimens.

The stoichiometric ratio s_c for oxidation of the char was derived from laminar-flow ablation tests. The best correlation curve was found to be[4]

$$q_C^*/H_e = 4.4 = (\rho_c s_c + \rho_g s_g)/\rho_v W_e + (\rho_c \eta_c + \rho_g \eta_g)_{\text{lam}}/\rho_v \quad (10)$$

The values assigned to W_e and η_{lam}, viz. 0.23 (neglecting contamination) and 0.70 (assuming combustion to CO) respectively, gave $s_c = 1.13$. Comparison with the theoretical value $s_c = 1.332$ for pure carbon indicated an effective carbon content of 85% in the R6300 char layer, and ΔH_c for the heterogeneous combustion of char to CO was reduced accordingly.

References

[1] Wakefield, R. M. and Lundell, J. H., "Comparison of the Performance of a Charring Ablator under Time-Varying and Constant Combined Convective and Radiative Heating," AIAA Paper 69-151, New York, 1969; *Journal of Spacecraft and Rockets*, Vol. 8, No. 6, June 1971, pp. 626–630.

[2] Comfort, E. H., "Ablation Measurements in Turbulent Flow," AIAA Paper 70-226, New York, 1970.

[3] "Avco Hyperthermal Simulation Capabilities," AVSD-0457-70-CA, Sept. 14, 1970, Avco Systems Div., Wilmington, Mass.

[4] Mitchel, B. J. and Tempesta, F. L., "Ablative Plastics Characterization, Part II. Trajectory Simulation," AFML-TR-67-176, Part II, Oct. 1968, Avco Space Systems Div., Wilmington, Mass.

[5] Pfahl, R. C., Jr. and Dropkin, D., "Thermocouple Temperature Perturbations in Low-Conductivity Materials," ASME Paper 66-WA/HT-8, ASME Winter Annual Meeting and Energy Systems Exposition, New York, Nov. 27–Dec. 1, 1966.

[6] Sparrow, E. M., Albers, L. U., and Eckert, E. R. G., "Thermal Radiation Characteristics of Cylindrical Enclosures," *Transactions of the ASME, Ser. C: Journal of Heat Transfer*, Vol. 84, No. 1, Feb. 1962, pp. 73–81.

[7] Beck, J. V. and Hurwicz, H., "Effect of Thermocouple Cavity on Heat Sink Temperature," *Transactions of the ASME, Ser. C: Journal of Heat Transfer*, Vol. 82, No. 1, Feb. 1960, pp. 27–36.

[8] Beck, J. V., "Calculation of Surface Heat Flux from an Internal Temperature History," ASME Paper 62-HT-46, *ASME-AIChE Heat Transfer Conference and Exhibit*, Houston, Texas, Aug. 5–8, 1962.

[9] Bartz, D. R., "A Simple Equation for Rapid Estimation of Rocket Nozzle Convective Heat Transfer Coefficients," *Jet Propulsion*, Vol. 27, No. 1, Jan. 1957, pp. 49–51.

[10] Katsikas, C. J., Castle, G. K., and Higgins, J. S., "Ablation Handbook: Entry Materials Data and Design," AFML TR 66-262, Nov. 1966, Avco Space Systems Div., Wilmington, Mass., pp. 31–63.

[11] Barriault, R. J. and Yos, J., "Analysis of the Ablation of Plastic Heat Shields that Form a Charred Surface Layer," *ARS Journal*, Vol. 30, No. 9, Sept. 1960, pp. 823–829.

[12] Bethe, H. A. and Adams, M. C., "A Theory for the Ablation of Glassy Materials," *Journal of the Aerospace Sciences*, Vol. 26, No. 6, June 1959, pp. 321–329.

[13] Mitchel, B. J., Pfahl, R. C., Jr., and Recesso, J. V., "Ablative Plastics Characterization, Part II. Critical Environments," AFML TR 65-156, Part II, June 1966, Avco Space Systems Div., Wilmington, Mass.

[14] Pfahl, R. C., Jr. and Mitchel, B. J., "Simultaneous Measurement of Six Thermal Properties of a Charring Plastic," *International Journal of Heat and Mass Transfer*, Vol. 13, No. 2, Feb. 1970, pp. 275–286.

[15] Katsikas, C. J., Castle, G. K., and Higgins, J. S., "Ablation Handbook: Entry Materials Data and Design," AFML TR 66-262, Nov. 1966, Avco Space Systems Div., Wilmington, Mass., pp. 349–363.

[16] Katsikas, C. J., Castle, G. K., and Higgins, J. S., "Ablation Handbook: Entry Materials Data and Design," AFML TR 66-262, Nov. 1966, Avco Space Systems Div., Wilmington, Mass., pp. 157–177.

[17] Ladacki, M., Hamilton, J. V., and Cohz, S. N., "Heat of Pyrolysis of Resin in Silica-Phenolic Ablator," *AIAA Journal*, Vol. 4, No. 10, Oct. 1966, pp. 1798–1802.

[18] Madorsky, S. L., *Thermal Degradation of Organic Polymers*, Interscience Publishers, Wiley, New York, 1964, pp. 288–292.